

Adipose-derived stem cell-mediated alphastatin targeting delivery system inhibits angiogenesis and tumor growth in glioma

CHEN LIANG¹, TING WEI², TING ZHANG³ and CHEN NIU⁴

Departments of ¹Neurosurgery, ²Ophthalmology and ³Otorhinolaryngology-Head and Neck Surgery; ⁴Positron Emission Tomography/Computed Tomography Center, First Affiliated Hospital of Xi'an Jiaotong University, Xi'an, Shaanxi 710061 P.R. China

Received May 16, 2023; Accepted September 13, 2023

DOI: 10.3892/mmr.2023.13102

Abstract. Malignant glioma is a highly vascularized tumor. Therefore, inhibition of angiogenesis is an effective treatment strategy for it. Alphastatin is a 24-amino acid peptide that has been demonstrated to inhibit glioma angiogenesis and tumor growth. Adipose-derived stem cells (ADSCs) are considered an ideal targeted drug delivery system for glioma therapy due to their targeted tropism for cancer and the intrinsic attribute of autologous transplantation. The aim of the present study was to construct an ADSC-mediated alphastatin targeted delivery system and investigate its effects on angiogenesis in glioma. The sequence encoding the human neurotrophin-4 signal peptide and alphastatin fusion gene fragment was transferred into ADSCs using a lentiviral vector to construct the ADSC-mediated alphastatin targeted delivery system (AI-ADSCs). Flow cytometry was used to detect the stem cell surface markers of AI-ADSCs. Western blot analysis and ELISA were used to detect the expression and secretion of alphastatin peptide in AI-ADSCs. Cell migration assay was used to detect the tendency of AI-ADSCs to target CD133⁺ glioma stem cells (GSCs). The effects of AI-ADSCs on angiogenesis *in vitro* were detected by tube formation assay. A Cell Counting Kit-8 assay was used to detect the effects of AI-ADSCs on endothelial cell (EC) proliferation. Wound healing assay was used to examine the effects of AI-ADSCs on EC migration. Intracranial xenograft models were constructed and *in vivo* fluorescence imaging was used to examine the effects of AI-ADSCs on glioma growth.

Fluorescence microscopy was used to detect the distribution of AI-ADSCs in glioma tissue and CD133 immunofluorescence staining was used to detect the effects of AI-ADSCs on GSCs in glioma tissue. The results revealed that ADSCs exhibited more marked tropism to GSCs than to other types of cells ($P < 0.01$). AI-ADSCs maintained the surface markers of ADSCs and there was no significant difference between the ADSCs and AI-ADSCs regarding tropism to GSCs ($P = 0.639$ for GSCs-SHG44 cells; and $P = 0.386$ for GSCs-U87 cells). AI-ADSCs were able to successfully secrete and express alphastatin peptide and inhibited EC-mediated angiogenesis ($P < 0.01$) and EC migration ($P < 0.01$) and proliferation ($P < 0.01$) *in vitro*. *In vivo*, AI-ADSCs were detected in glioma tissue and were able to inhibit tumor growth. In addition, the AI-ADSCs reduced the number of GSCs and microvascular density ($P < 0.01$) in the tumors. Overall, the results of the present study indicated that the AI-ADSCs were able to target glioma tissue and inhibit glioma angiogenesis and tumor growth. This anti-angiogenic targeted therapy system may provide a new strategy for the treatment of glioma.

Introduction

Despite improvements having been made to standard treatments, including surgery, radiotherapy and adjuvant chemotherapy, the prognosis of patients with malignant glioma remains poor (1). Therefore, the development of novel treatment strategies for glioma is crucial. Angiogenesis is a process through which new blood vessels are generated from pre-existing vessels and this process plays a critical role in the development and progression of human malignancies such as glioma (2). Malignant glioma is considered one of the most extensively vascularized types of tumor (3). Therefore, anti-angiogenesis therapy appears to be a promising treatment strategy for malignant glioma (4).

Previous research has found that fibrinogen E fragment, formed by plasmin cleavage of human fibrinogen, has an antiangiogenic effect, which is mainly associated the first 24 amino acids of the α chain of human fibrinogen contained within it. This 24-amino acid peptide is called alphastatin (5). A previous study confirmed that alphastatin could inhibit both the migration and tube formation of endothelial cells (ECs) induced by VEGF or basic fibroblast growth factor (bFGF)

Correspondence to: Professor Chen Liang, Department of Neurosurgery, First Affiliated Hospital of Xi'an Jiaotong University, 277 Yanta West Road, Xi'an, Shaanxi 710061, P.R. China
E-mail: liangchen01@xjtu.edu.cn

Professor Chen Niu, Positron Emission Tomography/Computed Tomography Center, First Affiliated Hospital of Xi'an Jiaotong University, 277 Yanta West Road, Xi'an, Shaanxi 710061, P.R. China
E-mail: niuchen.xjtu@mail.xjtu.edu.cn

Key words: adipose-derived stem cell, alphastatin, drug delivery system, angiogenesis, glioma

in vitro and inhibit glioma growth by inhibiting angiogenesis *in vivo* (6). The mechanism of the anti-angiogenic effect of alphastatin involves blocking the JNK and ERK phosphorylation pathways at the initial stage of angiogenesis and subsequent inhibition of EC migration and differentiation (6). In addition, alphastatin exhibits selective cytotoxicity on activated ECs in tumor blood vessels, which could cause extensive thrombosis of tumor blood vessels and lead to tumor necrosis (5). Notably, alphastatin selectively disrupts activated ECs in tumor vessels but has no detectable effect on vessels in normal tissues such as liver, lungs and kidneys, indicating its potential therapeutic effect for specifically targeting tumor angiogenesis (5). Therefore, alphastatin appears to be a safe and effective anti-angiogenic agent. However, to maximize the efficacy of alphastatin, it is essential to identify the appropriate method of administration of this molecule.

In recent years, the drug delivery system (DDS) has exhibited tremendous promise for enhancing the therapeutic effects of drugs. DDS can significantly enhance the pharmaceutical effects of drugs and can reduce the side effects of therapeutics in the treatment of various disease conditions (7). Compared with traditional DDS, cell-mediated DDS has numerous advantages, such as circulating in the bloodstream for a period of time, abundant surface ligands, targeting tumor cells and flexible morphology through biological barriers due to its unique cellular properties (8). Among all cell-mediated DDSs, the unique biological characteristics of mesenchymal stem cells (MSCs) make them valuable cytoreagents for tumor gene therapy. MSCs can relatively easily introduce and persistently express markers and/or therapeutic genes. MSCs can be directly obtained from patients and cultured and expanded *in vitro*, thus avoiding the immune rejection and ethical concerns caused by the use of allogeneic stem cells (9). Notably, their ability to migrate to tumor tissue makes them an ideal delivery vehicle for tumor treatment (8).

As a type of MSCs, adipose-derived stem cells (ADSCs) are isolated from human adipose tissue and are characterized by their morphology, surface markers and their potential to differentiate into mesenchymal and neuronal lineages (10). ADSCs have been demonstrated to be attractive cellular vehicles for gene therapy against malignancies due to their targeted tropism for cancer and the intrinsic attribute of autologous transplantation (11). In addition to the above advantages of MSCs, the success rate of ADSC isolation can reach 100% and the yield of ADSCs is ~40-fold higher than that of bone marrow-derived MSCs (11). Therefore, ADSCs can be easily prepared and genetically modified as targeting DDS for glioma therapy (12). In summary, ADSCs have advantages such as tumor tropism, wide availability, easy accessibility and low immunogenicity, making it an ideal tumor targeted drug delivery system.

The present study constructed an ADSC-mediated alphastatin targeted delivery system and investigated its effects on angiogenesis and tumor growth in glioma.

Materials and methods

Materials. The U87 MG American Type Culture Collection (ATCC) human glioblastoma cell line of unknown origin (cat no. CL-0238), SHG-44 human glioma cell line

(cat no. CL-0207), 293T cell line (cat no. CL-0005) and human umbilical vein endothelial cell line (HUVEC; cat no. CL-0122) were purchased from Procell Life Science & Technology Co., Ltd. The SVG p12 human astroglia cell line (cat no. CRL-8621) was purchased from the ATCC. The HUVECs used in the present study were not primary cells. Suppliers have authenticated all the aforementioned cell lines by short tandem repeat profiling. ADSCs (cat no. HUXMD-01001) were purchased from Cyagen Biosciences, Inc. A total of 15 male, 6-week-old, specific pathogen-free, BALB/C nude mice, weighing 16-18 g, were purchased from Changzhou Cavens Laboratory Animal Co., Ltd., and were housed in a full-barrier rodent facility with a filtered air supply at constant temperature (25°C) and humidity (50%) under a 12-h light/dark cycle. Water and food for animals were provided *ad libitum*. The housing environment for animals, water and animal feeds were sterilized. All animal procedures were performed in accordance with the guidance of the Research Ethics Committee of The First Affiliated Hospital of Xi'an Jiaotong University (approval number: 2020-G-263).

Cell culture. The U87, SHG44, 293T and SVG p12 cells were cultured in Dulbecco's modified Eagle's medium (Gibco; Thermo Fisher Scientific, Inc.) supplemented with 10% fetal bovine serum (Gibco; Thermo Fisher Scientific, Inc.). HUVECs were cultured in F12K medium (Procell Life Science & Technology Co., Ltd.) supplemented with 10% fetal bovine serum. ADSCs were cultured in human adipose-derived stem cell growth medium (cat. no. HUXMD-90011; Cyagen Biosciences, Inc.). All cells were cultured in an atmosphere of 5% CO₂ at 37°C.

Construction and transfection of alphastatin lentivirus. The lentiviral vector plasmid pLVX-mCMV-ZsGreen-IRES-Puro was purchased from Wuhan Viraltherapy Technologies Co., Ltd. The pUC57-NT4-alphastatin plasmid containing the sequence encoding the human neurotrophin-4 (NT4) signal peptide and alphastatin fusion gene fragment (NT4-AI) and FLAG tag was synthesized and purchased from GenScript. The NT4-AI-FLAG sequence was cloned into pLVX-mCMV-ZsGreen-IRES-Puro and identified by restriction enzyme digestion and sequence analysis. Lentiviral particles were produced by the transfection of 293T cells with a lentivirus packaging kit (cat. no. R003; Wuhan Viraltherapy Technologies Co., Ltd.) according to the manufacturer's instructions and lentiviral supernatants were collected after 48 h. The construction of negative control (NC) lentivirus was performed as described above. ADSCs were seeded in 24-well plates at a concentration of 5×10⁴ cells/well and infected with concentrated alphastatin lentiviral particles (AI-ADSCs) or NC lentiviral particles (NC-ADSCs; multiplicity of infection=20) in an atmosphere of 5% CO₂ at 37°C for 24 h. Successful transfection of cells was verified by expression of green fluorescent protein.

Detection of MSC surface markers in transfected ADSCs. Flow cytometric detection of MSC surface markers was used to determine whether lentivirus transfection affected the biological characteristics of ADSCs. AI-ADSCs, NC-ADSCs and ADSCs were seeded in six-well plates at a concentration

of 5×10^5 cells/well and cultured in an atmosphere of 5% CO₂ at 37°C for 48 h. The cells were then quantified using a cell counting board and resuspended with 0.1 ml phosphate-buffered saline (PBS) containing 0.5% bovine serum albumin (BSA; Thermo Fisher Scientific, Inc.). Allophycocyanin (APC)-conjugated anti-human CD13 antibody (cat. no. 301705; BioLegend, Inc.), APC-conjugated anti-mouse/human CD44 antibody (cat. no. 103011; BioLegend, Inc.), phycoerythrin (PE)/Cyanine7-conjugated anti-human CD90 (Thy1) antibody (cat. no. 328123; BioLegend, Inc.) and PE-conjugated anti-human CD105 (endoglin) antibody (cat. no. 12-1057-41; eBioscience; Thermo Fisher Scientific, Inc.) were added according to the manufacturer's instructions. Following incubation at 4°C for 30 min, the cells were washed twice with PBS containing 0.5% BSA. A single cell suspension was prepared by the addition of 0.2 ml PBS and stem cell surface markers were then detected using flow cytometry (CytoFLEX; Beckman Coulter, Inc.) and CytExpert 2.4 software (Beckman Coulter, Inc.).

Western blot analysis. The expression level of alphastatin was detected indirectly by detecting the expression of the FLAG tag. Extraction of total cellular proteins and western blot analysis were performed as previously described (13). Briefly, cells were washed twice with PBS and lysed on ice following the addition of 300 μ l RIPA buffer (Beyotime Institute of Biotechnology) with 1 mmol/l phenylmethylsulfonyl fluoride. Protein concentration was determined using a bicinchoninic acid protein assay kit (Beyotime Institute of Biotechnology). Protein samples (40 μ g) were boiled in 1X SDS-PAGE sample loading buffer, resolved using 10% SDS-PAGE and transferred onto polyvinylidene fluoride membranes (MilliporeSigma). The membranes were then blocked with TBS-0.1% Tween-20 (TBST) containing 5% non-fat dry milk at room temperature for 2 h and probed with primary antibodies overnight at 4°C, followed by incubation with secondary antibodies conjugated to horseradish peroxidase at 37°C for 2 h. Membranes were developed using SuperSignal West Pico PLUS Chemiluminescent Substrate (Thermo Fisher Scientific, Inc.). The primary antibodies employed in western blotting were as follows: Goat anti-FLAG tag antibody (1:1,000; cat. no. ab1257; Abcam) and rabbit anti-GAPDH antibody (1:5,000; cat. no. ap0063, Bioworld Technology, Inc.). The secondary antibodies employed in western blotting were as follows: HRP-conjugated goat anti-rabbit immunoglobulin G (IgG) antibody (1:5,000; cat. no. BA1054) for GAPDH detection and HRP-conjugated rabbit anti-goat IgG antibody (1:5,000; cat. no. BA1060) for FLAG tag detection (both from Wuhan Boster Biological Technology, Ltd.). ImageJ 1.8 software (National Institutes of Health) was used for densitometry.

Measurement of alphastatin secretion from ADSCs. The secretion levels of alphastatin from alphastatin lentivirus-transfected ADSCs (AI-ADSCs) were assessed using a FLAG tag protein ELISA kit (cat. no. E4700-100; BioVision, Inc.). Briefly, the supernatant of ADSCs in each group was collected at 48 h following infection with lentivirus. The samples were centrifuged at room temperature for 20 min at 850 x g to remove particulates and were immediately assayed

using the aforementioned kit according to the manufacturer's instructions.

Isolation of CD133⁺ glioma stem cells (GSCs). U87 and SHG44 cells were resuspended in 1 ml PBS containing 0.5% BSA in an Eppendorf tube containing with 1×10^6 cells per tube. Following centrifugation (200 x g for 3 min at 4°C), the cells were washed with PBS containing 0.5% BSA once and then incubated with 5 μ l anti-CD133 antibody (cat. no. 17-1338-42; Invitrogen; Thermo Fisher Scientific, Inc.) at 4°C for 30 min. Subsequently, the cells were washed twice with PBS containing 0.5% BSA and resuspended for cell sorting using a flow cytometer (FACSaria III; BD Biosciences).

In vitro analysis of tropism of transfected ADSCs to GSCs. Cell migration assay was used to analyze the tropism of AI-ADSCs to GSCs *in vitro*. Transwell chambers (cat. no. 353097; BD Biosciences) with 8- μ m pore size polyethylene terephthalate (PET) membranes were placed in 24-well plates (Corning, Inc.). GSCs, CD133⁺ glioma cells or SVG p12 cells were seeded in the lower chambers (2.5×10^5 cell/well) and cultured overnight in an atmosphere of 5% CO₂ at 37°C. Cell suspension of AI-ADSCs, NC-ADSCs or ADSCs (3×10^5 cells/ml) was then added to the upper chambers (200 μ l/well) and co-cultured with cells in the lower chamber in an atmosphere of 5% CO₂ at 37°C overnight. The migrated cells adhering to the bottom surface of the membranes were fixed with a 70% ethanol solution at 4°C for 1 h and stained with 0.5% crystal violet (cat. no. C0121; Beyotime Institute of Biotechnology) at room temperature for 10 min. The migrated cells were then counted under an optical microscope (IX51; Olympus Corporation; magnification, x200).

In vitro tube formation assay. The effect of AI-ADSCs on the angiogenesis of ECs was analyzed using a tube formation assay *in vitro*. Matrigel (cat. no. 356234; Corning, Inc.) was incubated at 4°C for 24 h and then 0.1 ml Matrigel was evenly plated onto 24-well plates (Corning, Inc.), precooled at -20°C for ≥ 10 min and then incubated for 30 min at 37°C. Subsequently, HUVECs (1.5×10^5 cells/well) were seeded onto the Matrigel-coated plates and incubated in an atmosphere of 5% CO₂ at 37°C for 2.5 h. Transwell chambers (cat. no. 353095; BD Biosciences) with 0.4- μ m pore size PET membranes were then placed in the 24-well plates and a cell suspension of AI-ADSCs, NC-ADSCs or ADSCs (3×10^5 cells/ml) was added to the Transwell chambers (200 μ l/well). The cells in the upper and lower chambers were co-cultured in an atmosphere of 5% CO₂ at 37°C for 8 h. The EC-derived tube-like structures in each well were visualized and analyzed directly under an optical microscope (IX51; Olympus Corporation; magnification, x100).

EC scratch wound healing assay. A scratch wound healing assay was used to examine the effects of AI-ADSCs on the migration of ECs. The HUVECs were seeded at a density of 5×10^5 cells/well in six-well plates. After 24 h, the cell monolayer was scraped in a straight line using a 20- μ l pipette tip and the cells were washed three times with PBS. Transwell chambers (cat. no. 353090; BD Biosciences) with 0.4- μ m pore size PET membranes were then placed in the six-well plates

and a cell suspension of AI-ADSCs, NC-ADSCs or ADSCs (5×10^5 cells/well) was added to the Transwell chambers. The cells in the upper and low chambers were co-cultured in serum-free medium in an atmosphere of 5% CO₂ at 37°C for 24 h. Images of the plates were captured under an optical microscope (IX51; Olympus Corporation; magnification, x100) at 0 and 24 h, respectively. ImageJ 1.8 software (National Institutes of Health) was used to measure the migration area and the percentage of wound healing was calculated. The calculation method was $(\text{Area}_{0\text{h}} - \text{Area}_{24\text{h}}) / \text{Area}_{0\text{h}}$.

Cell Counting Kit-8 (CCK-8) cell proliferation assay. A CCK-8 kit (cat. no. E-CK-A362; Elabscience Biotechnology, Inc.) was used to examine the effect of AI-ADSCs on the proliferation of ECs. HUVECs were seeded at a density of 5×10^3 cells/well in 24-well plates. After 24 h, Transwell chambers (cat. no. 353095; BD Biosciences) with 0.4- μm pore size PET membranes were placed in the 24-well plates and a cell suspension of AI-ADSCs, NC-ADSCs or ADSCs (5×10^3 cells/well) was added to the Transwell chambers. The cells in the upper and low chambers were co-cultured in an atmosphere of 5% CO₂ at 37°C. The HUVECs in low chambers were then analyzed by CCK-8 assay at 24 and 48 h following co-culture. Briefly, 50 μl CCK-8 solution was added to each well. Following incubation at 37°C for 4 h, the absorbance at 450 nm was measured with a microplate reader (Flexstation 3; Molecular Devices, LLC).

Animal experiments. The establishment of intracranial xenograft models was conducted as previously described (14). The 15 BALB/C nude mice were randomly divided into three groups. To prevent accidental animal death, one additional mouse was added to each group. Each group of six mice was randomly numbered 1 to 6. The animals were anaesthetized with an intraperitoneal injection of 30 mg/kg pentobarbital sodium. U87 glioma cells transfected with LV-mCherry-Puromycin Lentivirus [cat. no. FLV050; Fubio (Suzhou) Biomedical Technology Co., Ltd.] and able to stably express a red fluorescent protein mCherry were injected intracranially using a stereotaxic apparatus (2.5 μl /mouse; cell concentration, 2×10^5 cells/10 μl). At day 3 after model establishment, a suspension of NC-ADSCs or AI-ADSCs (2.5 μl /mouse; cell concentration, 2×10^5 cells/10 μl) was injected into the periphery of the tumor modeling area. The number of intracranial injection cells followed the guidelines for the welfare and use of animals in cancer research (15). Animal health and behavior were monitored twice a week. After 28 days of tumor cell implantation, due to no accidental animal death, 5 mice numbered 1 to 5 in each group underwent subsequent experiments, while mice numbered 6 continued to be raised until the humane endpoint. The 15 tumor-bearing mice (5 mice/group) were sacrificed after observing intracranial tumorigenesis using an *in vivo* imaging instrument (IVIS Lumina III; PerkinElmer, Inc.) at 28 days following tumor cell implantation by an intraperitoneal injection of 200 mg/kg pentobarbital sodium solution. Cardiac arrest for 2 min was used to identify mortality. The humane endpoints included labored breathing, inability to remain upright, impaired mobility, a hunched posture for >48 h and no response to external stimuli. The mice were perfused with 4% paraformaldehyde for 1 h at 4°C

immediately following sacrifice, before the brain and tumor samples were obtained and fixed overnight with 4% paraformaldehyde at 4°C. Paraffin-embedded sections were prepared of a thickness of 4 μm . Briefly, the tissues were dehydrated by serial incubations in 75% alcohol (4 h), 85% alcohol (2 h), 90% alcohol (1.5 h), 95% alcohol and 100% alcohol (2 times, 0.5 h each). The tissues were then washed in a 1:1 mixture of 100% alcohol and xylene (10 min) and xylene (2 times, 10 min each). After washing, the tissues were immersed in paraffin (3 times, 1 h each) and then embedded in paraffin blocks. The distribution of NC-ADSCs or AI-ADSCs was observed under a fluorescence microscope (BX53; Olympus Corporation).

Detection of CD133⁺ GSCs in the xenograft model. CD133 immunofluorescence staining was used to detect CD133⁺ GSCs in the xenograft model. Sections were incubated overnight with an anti-CD133 antibody (cat. no. 66666-1-IG; Proteintech Group, Inc.) diluted 1:100 at 4°C. The NC sections were incubated with PBS instead of the antibody. After washing, the sections were incubated with cyanine 3-conjugated goat anti-mouse IgG (cat. no. BA1031; Wuhan Boster Biological Technology, Ltd.) diluted 1:100 at 37°C for 1 h. The CD133⁺ GSCs were observed under a fluorescence microscope (BX53; Olympus Corporation).

Microvessel density (MVD) detection in xenograft models. CD34 staining was performed to detect MVD. All procedures were performed according to the manufacturer's protocols. The sections were incubated overnight at 4°C with a rabbit anti-CD34 antibody (1:200; cat. no. ab81289; Abcam). The NC sections were incubated with PBS instead of the antibody. Antibody localization was determined using a 3,3'-diaminobenzidine substrate kit (Wuhan Boster Biological Technology, Ltd.). MVD was evaluated by detecting the cluster of CD34⁺ cells. Briefly, the tumor sections were scanned at low magnifications (x40 or x100) to determine the areas of most intense tumor angiogenesis, termed 'hot spots'. Following 'hot spot' identification, the MVD was calculated by averaging the number of individual microvessels in five fields under an optical microscope (IX51; Olympus Corporation) at high magnification (x400).

Statistical analysis. Data are presented as the mean \pm standard deviation of three replicates and analyzed using SPSS 17.0 software (SPSS, Inc.). One-way analysis of variance was used to compare the groups and the least significant difference post hoc test (≤ 3 groups) or Tukey's test (> 3 groups) were performed to further determine inter-group comparisons. $P < 0.05$ was considered to indicate a statistically significant difference.

Results

Construction of an ADSC-mediated alphastatin targeted delivery system. As presented in Fig. 1, following transfection with alphastatin lentivirus (Fig. 1A), the FLAG tag protein could be detected in AI-ADSCs, which indicated that the AI-ADSCs expressed alphastatin. No alphastatin expression was detected in the control or NC groups (Fig. 1C). In addition, FLAG tag protein could be detected in the supernatant of

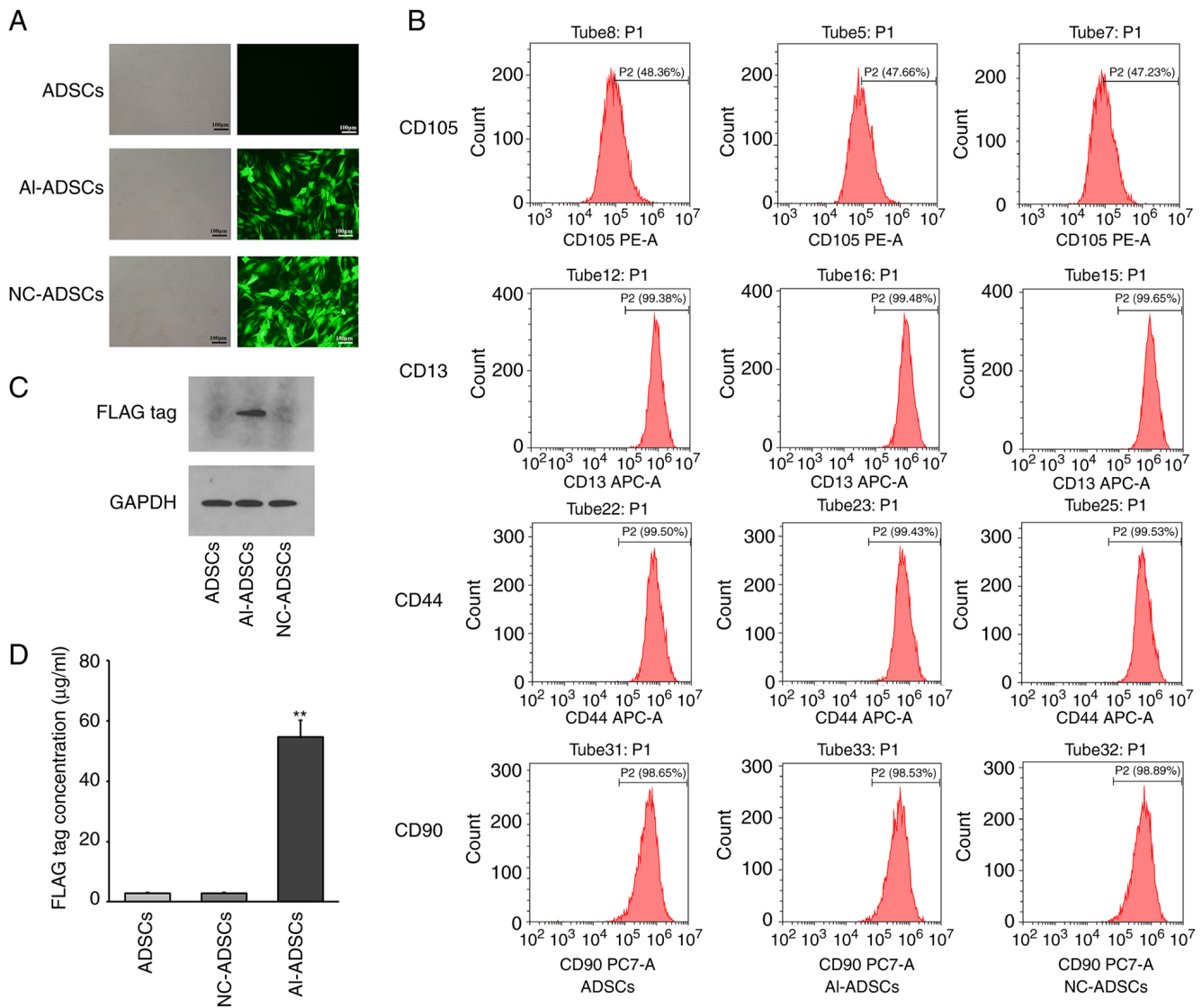


Figure 1. Construction and identification of an ADSC-mediated AI-ADSCs. (A) Construction of an ADSC-mediated AI-ADSCs and negative control-ADSCs using lentivirus infection. The stably transfected cells expressed green fluorescent protein. Scale bars, 100 μm . (B) AI-ADSCs expressed mesenchymal stem cell surface markers. (C) AI-ADSCs expressed FLAG tag protein. (D) FLAG tag protein was detected in the supernatant of AI-ADSCs. ** $P < 0.01$ vs. ADSCs. ADSCs, adipose-derived stem cells; AI, alphastatin; AI-ADSCs, alphastatin targeted delivery system.

AI-ADSCs using ELISA, which demonstrated that AI-ADSCs had the function of exocrine alphastatin secretion (Fig. 1D). Compared with the ADSCs, there was no significant difference in the expression of MSC surface markers, including CD13, CD44, CD90 and CD105, in AI-ADSCs, which indicated that alphastatin lentiviral transfection had no significant effect on the stem cell characteristics of ADSCs (Fig. 1B).

Isolation of GSCs and tropism of ADSCs to GSCs. As presented in Fig. 2, GSCs were isolated from U87 and SHG44 glioma cell lines using flow cytometry (Fig. 2B). Cell migration assay revealed that ADSCs exhibited more obvious tropism to GSCs than to CD133⁺ glioma or SVG p12 cells ($F=708.439$; $P=0.001$; Fig. 2A and C). There was no significant difference between ADSCs, NC-ADSCs or AI-ADSCs regarding tropism to GSCs ($F=0.484$; $P=0.639$ for GSCs-SHG44; and $F=1.122$; $P=0.386$ for GSCs-U87; Fig. 2D), which indicated that alphastatin lentiviral transfection had no significant effect on the tropism of ADSCs to GSCs.

Effects of ADSC-mediated alphastatin targeted delivery system on ECs *in vitro*. As presented in Fig. 3, tube formation assay revealed that AI-ADSCs significantly inhibited the angiogenesis of HUVECs *in vitro* ($F=98.262$; $P=0.001$; Fig. 3C and D). Scratch wound healing assay revealed that the wound healing ability of the HUVECs decreased following coculture with AI-ADSCs, suggesting that the AI-ADSCs inhibited HUVEC migration ($F=554.852$; $P=0.001$; Fig. 3A and B). In addition, cell proliferation assay revealed that the proliferation of HUVECs was inhibited by AI-ADSCs. At 48 h following co-culture with AI-ADSCs, the absorbance of HUVECs at 450 nm was lower than that of the control group, indicating that AI-ADSCs significantly inhibited the proliferation of HUVECs ($F=310.614$; $P=0.001$; Fig. 3E and F). Notably, the ADSCs and NC-ADSCs exerted promoting effects on the proliferation, migration and tube formation abilities of HUVECs *in vitro*.

Effects of ADSC-mediated alphastatin targeted delivery system on the glioma xenograft model. As presented in Fig. 4, both

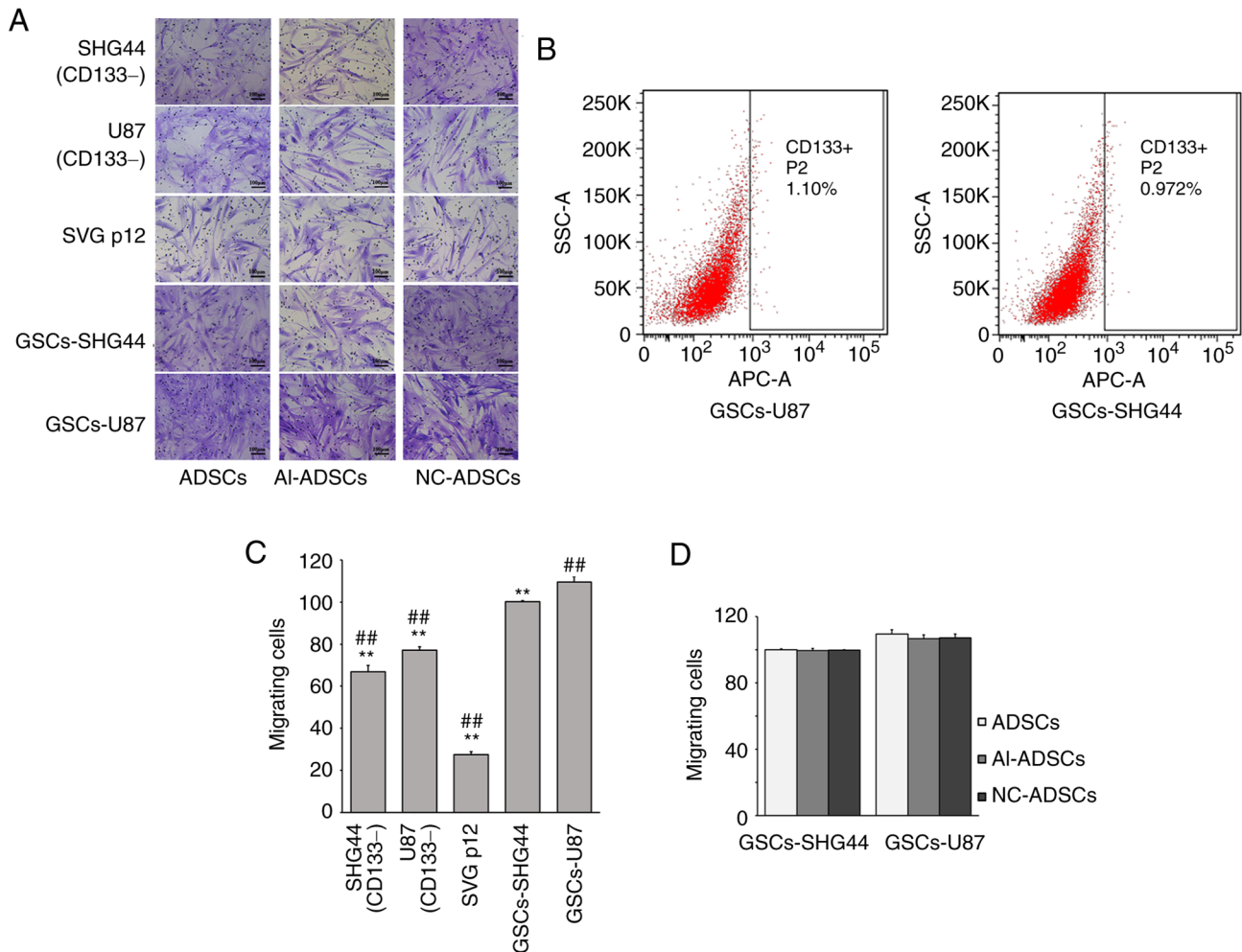


Figure 2. *In vitro* analysis of the tropism of the ADSC-mediated AI-ADSCs to GSCs. (A) Tropism of the ADSC-mediated AI-ADSCs to different cell types. Scale bars, 100 μ m. (B) Isolation of GSCs using flow cytometry. (C) Number of AI-ADSCs migrating to different cell types. ** $P < 0.01$ vs. the GSCs-U87 group; ## $P < 0.01$ vs. GSC-SHG44 group. (D) Number of ADSCs migrating to GSCs before and after lentiviral transfection. ADSCs, adipose-derived stem cells; AI, alphastatin; AI-ADSCs, alphastatin targeted delivery system; GSCs, glioma stem cells.

NC-ADSCs and AI-ADSCs were detected in glioma xenograft tissue using a fluorescence microscope (Fig. 4B), which indicated that AI-ADSCs could migrate into tumor tissue. *In vivo* imaging revealed that the AI-ADSCs significantly inhibited tumor growth in the glioma xenograft model. Furthermore, the number of CD133⁺ cells in the AI-ADSC group was significantly reduced (Fig. 4A). Immunohistochemical assay revealed that AI-ADSCs significantly reduced the MVD in glioma xenograft tissue ($F=16.236$; $P=0.001$; Fig. 4C).

Discussion

Alphastatin has been confirmed to exert an antitumor effect in several tumor models, such as gastric cancer (16), mammary carcinoma (17) and glioma (6,18). The antitumor effect of alphastatin is mainly due to its anti-angiogenic effect. Alphastatin can not only inhibit new vessel growth, but can also significantly lead to the regression of existing tumor vessels (18). Although alphastatin has been shown to exert an effective antitumor effect in previous studies (6,18), it is necessary to identify an appropriate method of administration in order to maximize its effect. In previous studies,

lentivirus-mediated gene transfer was used to express alphastatin in HUVECs and human glioma cell lines (6,18). Since the alphastatin sequence alone is not sufficient for efficient expression and secretion in mammalian cells, the alphastatin coding sequence should be fused to a signal peptide sequence to allow sufficient secretion of expressed alphastatin. At present, the NT4 signal peptide is one of the commonly used signal peptides for the construction of secreted and expressed peptide fusion genes. We successfully fused the NT4 signal peptide and pro-region sequence to the alphastatin coding sequence (NT4-AI) in our previous research and verified its expression effect (19). Therefore, the present study continued to use this fusion gene as the expression sequence of alphastatin. It has been demonstrated that the recombinant lentivirus-mediated NT4-AI gene delivery system of alphastatin can significantly suppress tumor growth and tumor angiogenesis in a xenograft glioma model (6,18). In the present study, a lentiviral vector carrying the NT4-AI fusion gene was used to infect ADSCs to construct an ADSC-mediated alphastatin targeted delivery system. The results revealed that NT4-AI lentiviral transfection did not affect the stem cell characteristics of ADSCs or the tropism to GSCs. At the same time, the ADSCs transfected

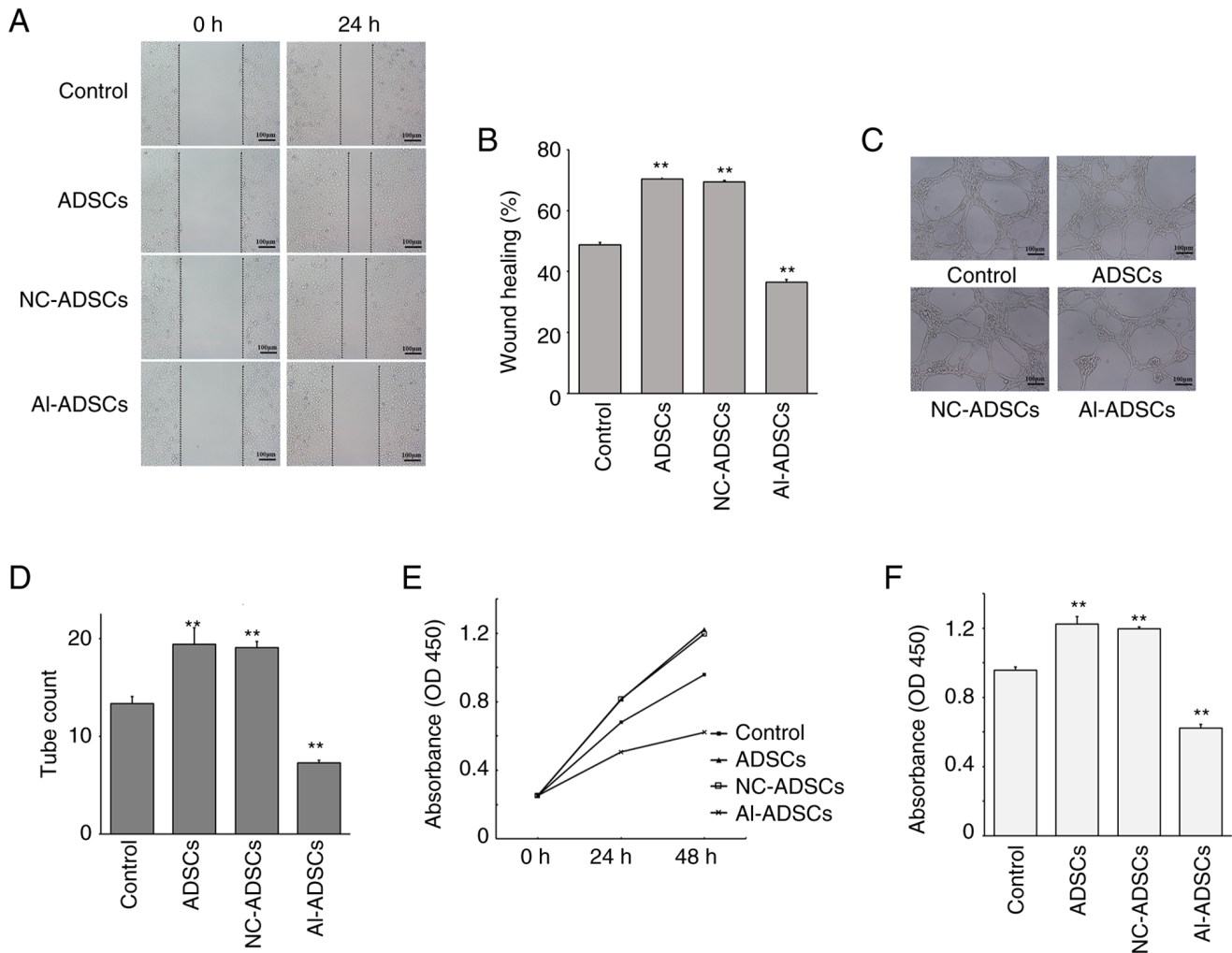


Figure 3. Effects of the ADSC-mediated AI-ADSCs on endothelial cells *in vitro*. (A) The results of the scratch wound healing assay in each group are presented. Scale bars, 100 μ m. (B) The percentage of wound healing in each group. ** $P < 0.01$ vs. the control group. (C) Results of tube formation assay for each group. Scale bars, 100 μ m. (D) The tube counts in each group are shown. ** $P < 0.01$ vs. the control group. (E) HUVEC proliferation curve was plotted based on the absorbance value at 450 nm. (F) Absorbance of HUVECs at 450 nm following co-culture with AI-ADSCs for 48 h. ** $P < 0.01$ vs. the control group. ADSCs, adipose-derived stem cells; AI, alphastatin; AI-ADSCs, alphastatin targeted delivery system; HUVEC, human umbilical vein endothelial cell; NC, negative control.

with NT4-AI lentivirus significantly expressed and secreted alphastatin. These results indicated that an ADSC-mediated alphastatin targeted delivery system was successfully constructed.

Subsequently, the present study examined the effects of the ADSC-mediated alphastatin targeted delivery system on EC proliferation, migration and angiogenesis *in vitro*. The results revealed that the ADSC-mediated alphastatin targeted delivery system significantly inhibited the angiogenesis, migration and proliferation of ECs *in vitro*. Previous studies have shown that alphastatin inhibits the migration and tubule formation of ECs mediated by VEGF or bFGF (5,6,18). As VEGF and bFGF do not bind to alphastatin directly (5), it is hypothesized that antiangiogenic activity of alphastatin probably operates at a post-receptor locus common to the VEGF and bFGF signaling pathways. MAPK signals have been reported to be involved in VEGF and bFGF mediated EC proliferation, migration, differentiation and lumen formation. Among them, activation of the ERK-MAPK pathway can promote endothelial cell proliferation, while the JNK-MAPK pathway plays an important role in

both EC proliferation and migration (20). Our previous study confirmed that alphastatin attenuated the VEGF or bFGF induced phosphorylation of JNK and ERK at the initial stage of angiogenesis, thus inhibiting the proliferation and migration of ECs and ultimately inhibiting angiogenesis (6). A further study suggested that alphastatin inhibited the downregulation of vascular endothelial cadherin (VE-cadherin) on the surface of EC induced by VEGF or bFGF, which led to the turnover of VE-cadherin on the EC membrane (18). VE-cadherin is an adhesion molecule crucial for vascular integrity and endothelial cell survival (21). VE-cadherin turnover on the EC membrane can suppress angiogenesis and is closely related to the MAPK pathways (22). Therefore, our previous data suggest that the anti-angiogenic mechanism of alphastatin is partially achieved by inhibiting the activation of JNK and ERK kinases and blocking the VEGF and bFGF signaling pathways, leading to VE cadherin turnover in ECs and then inhibiting EC migration and differentiation, thus inhibiting angiogenesis. In addition, the inhibition of angiogenesis by alphastatin also involves the sphingosine kinase/sphingosine-1-phosphate

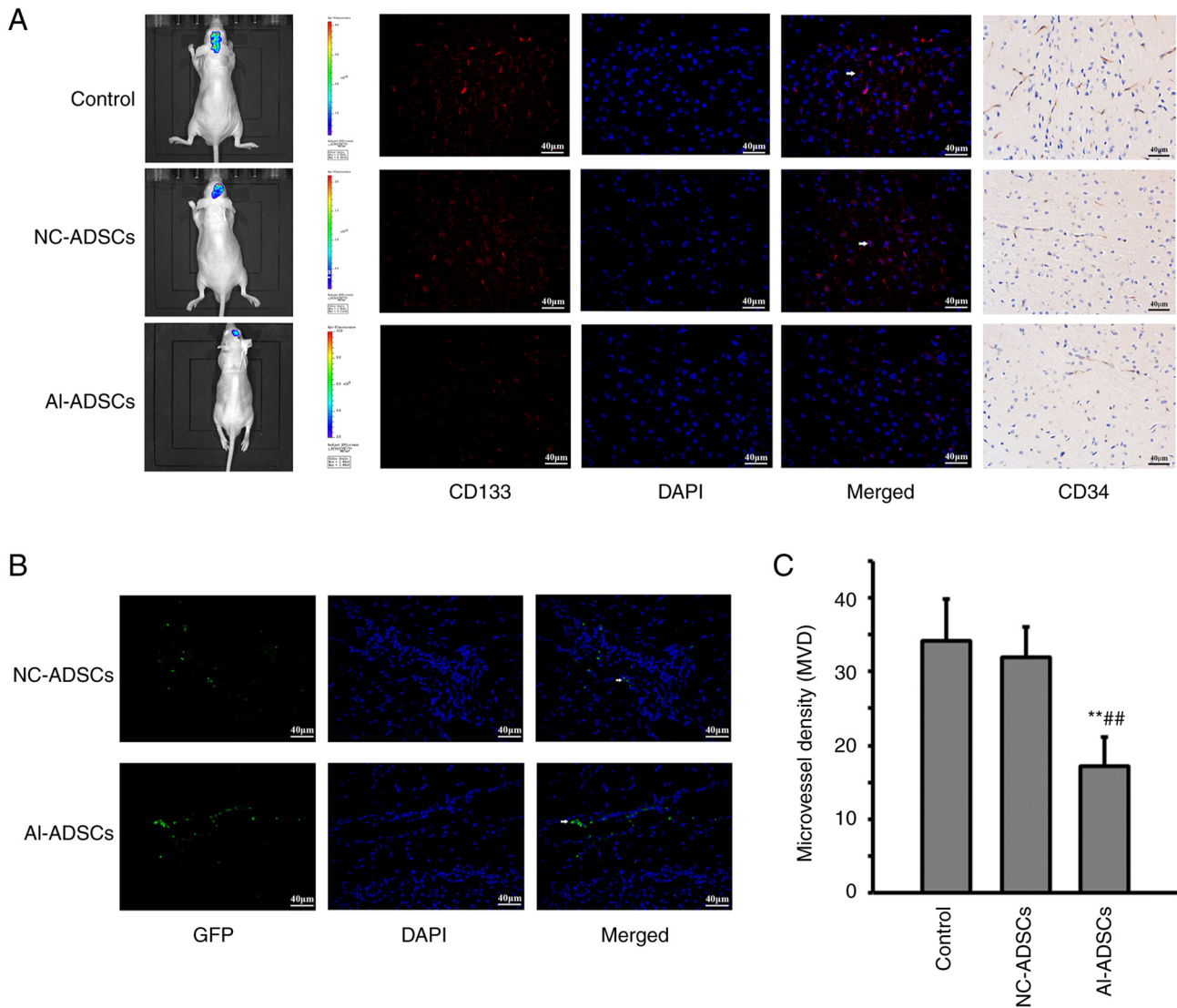


Figure 4. Effects of the ADSC-mediated Al-ADSCs on a glioma xenograft model. (A) *In vivo* imaging, CD133 immunofluorescence staining and CD34 immunohistochemical staining in each group. White arrows represent the Al-ADSCs CD133⁺ GSCs. Scale bars, 40 μ m. (B) Al-ADSCs and NC-ADSCs (expressing green fluorescent protein) in tumor tissue. White arrows represent the Al-ADSCs or NC-ADSCs. Scale bars, 40 μ m. (C) Microvessel density in each group. ** $P < 0.01$ vs. the control group; ## $P < 0.01$ vs. the NC-ADSCs group. ADSCs, adipose-derived stem cells; Al, alphastatin; Al-ADSCs, alphastatin targeted delivery system; NC, negative control.

(SPK/S1P) signaling pathway. It has been confirmed that the SKP/S1P signaling pathway is involved in the regulation of hepatocyte growth factor-induced EC migration (23) and also mediates the activation of the MAPK signaling pathway induced by VEGF (24), thus playing an important role in EC angiogenesis. Another study indicated that alphastatin decreases EC SPK activity and reduced S1P production, which inhibits the process of angiogenesis (16). However, the mechanism by which alphastatin inhibits endothelial cell angiogenesis may go beyond this. A previous study has shown that after alphastatin treatment, 29 proteins are significantly differentially expressed in ECs (25). Among them are nucleoside diphosphate kinase B (NDPKB) and profilin-2 (PFN2), which are involved in EC angiogenesis. NDPKB is essential for VEGF-induced angiogenesis and contributes to the correct localization of VEGF receptor type 2 and VE-cadherin at the endothelial adherens junctions (26). PFN2 promotes EC proliferation, migration and tube formation through the

phosphoinositide 3-kinase-PFN2-ERK axis (27). Alphastatin significantly inhibits the expression of NDPKB and PFN2 in EC (25), which may also be one of the possible mechanisms by which alphastatin inhibits EC angiogenesis. The above data indicate that the mechanism by which alphastatin inhibits angiogenesis is very complex and further research is needed.

In addition, the present study found that ADSCs promoted the proliferation, migration and tube formation abilities of ECs, which was consistent with previous findings (28,29). Of note, the present study demonstrated that alphastatin significantly inhibited these promoting effects of ADSCs on ECs. The promoting effect of ADSCs on ECs is mainly mediated through a variety of angiogenic factors contained in extracellular vesicles, such as VEGF (29), and alphastatin can inhibit the migration and differentiation of ECs in the presence of VEGF or bFGF (6). This may be one of the reasons why it can inhibit ADSC-mediated angiogenesis. However, the mechanisms involved warrant further investigation.

In animal experiments, the tropism of the ADSC-mediated alphastatin targeted delivery system to glioma *in vivo* was confirmed. ADSC can be chemotactically recruited into glioma (30). The stromal-derived factor-1/C-XC chemokine receptor type 4 axis plays a critical role in this innate tumor-homing ability of ADSCs (12). Previous studies have shown that ADSCs can be used as an effective drug targeted delivery system for glioma (31,32). In addition, the safety of the ADSC-mediated drug delivery system has also been preliminarily verified (31,33). The present study found that the ADSC-mediated alphastatin targeted delivery system could migrate into glioma tissue, which inhibited angiogenesis and tumor growth. Notably, the number of GSCs decreased significantly in tumors with the ADSC-mediated alphastatin targeted delivery system. GSCs reside in specialized niche where interaction with the microenvironment regulates their stem cell behavior (34). ECs in the GSC niche microenvironment play a key role in the maintenance and self-renewal of GSCs (35). Currently, there is no evidence to suggest that alphastatin can directly affect GSC. However, a previous study showed that disrupting the niche microenvironment by inhibiting angiogenesis can hinder the self-renewal of GSCs (36). Therefore, considering the inhibitory effect of alphastatin on EC proliferation, migration and angiogenesis, the reduction of GSCs may be associated with the interference of alphastatin of the interaction between ECs and GSCs in the GSC niche. The decreased number of GSCs can also affect tumor growth (37). Therefore, the mechanisms of the ADSC-mediated alphastatin targeted delivery system regarding the inhibition of glioma growth may be mediated via the suppression of tumor angiogenesis and GSCs. However, these mechanisms require further investigation.

As aforementioned, the inhibitory effect of alphastatin on tumor angiogenesis has been confirmed in previous studies. The present study innovatively established an ADSC-mediated alphastatin targeting delivery system. Through this system, the specific expression of alphastatin and its anti-angiogenesis effect in glioma tissue have been achieved, which has not been previously reported. In addition, the present study found that targeted anti-angiogenic strategy using ADSCs as carriers appeared to reduce the number of GSCs in glioma tissue, which has rarely been reported in previous studies. This appears to provide some new ideas for glioma treatment strategies targeting GSCs. In summary, the present study may provide a new strategy for the treatment of glioma.

As the ADSC-mediated alphastatin targeted delivery system is a new concept, there are currently no other studies that use this targeted delivery system to treat glioma or other types of tumors. Therefore, more research is needed to analyze its advantages and limitations in the treatment of tumors. However, there are still some noteworthy issues in this delivery system. First, exogenous therapeutic genes may affect the biological characteristics of ADSCs. Therefore, after introducing exogenous genes, it is necessary to evaluate the tumor tropism and stem cell characteristics of ADSCs. Second, before clinical application, the safety of this delivery system needs to undergo a more comprehensive and rigorous evaluation. Third, since the present study only observed the anti-glioma effect of the targeted delivery system for a relatively short period of time, its long-term efficacy needs further observation.

In conclusion, in the present study, an ADSC-mediated alphastatin targeted delivery system was constructed and its tumor tropism to glioma was confirmed *in vitro* and *in vivo*. Furthermore, this targeted delivery system was demonstrated to be able to express and secrete alphastatin, which inhibited angiogenesis and reduced the number of GSCs and inhibited tumor growth. These results indicated that the ADSC-mediated alphastatin targeted delivery system is a promising strategy for glioma treatment. However, since it is a preliminary study, the present study had certain limitations. First, it did not evaluate the effect of the ADSC-mediated alphastatin targeted delivery system on blood vessels in normal tissues throughout the body. Second, the underlying mechanisms by which this delivery system inhibits glioma angiogenesis, GSCs and tumor growth warrant further investigation. Furthermore, the present study did not directly detect alphastatin secreted by this targeted delivery system using methods such as time-of-flight mass spectrometry. These will be the focus of future research.

Acknowledgements

Not applicable.

Funding

The present study was supported by grants from Key Research and Development Plan of Shaanxi Province, China (grant no. 2023-YBSF-242), Natural Science Basic Research Program of Shaanxi (grant nos. 2019JQ-247 and 2022JQ-792) and National Natural Science Foundation of China (grant no. 82102014).

Availability of data and materials

The data used and/or analyzed during the current study are available from the corresponding author on reasonable request.

Authors' contributions

CL was responsible for writing the main manuscript and data analysis. CL and CN contributed to the study design. TW and TZ contributed to the molecular biology experiment and animal experiment. CL and CN confirm the authenticity of all the raw data. All authors have read and approved the final manuscript.

Ethics approval and consent to participate

The present study has been approved by the Research Ethics Committee of The First Affiliated Hospital of Xi'an Jiaotong University (approval no. 2020-G-263) and complies with the International Society for Stem Cell Research guidelines.

Patient consent for publication

Not applicable.

Competing interests

The authors declare that they have no competing interests.

References

1. Stupp R, Lukas RV and Hegi ME: Improving survival in molecularly selected glioblastoma. *Lancet* 393: 615-617, 2019.
2. Ahir BK, Engelhard HH and Lakka SS: Tumor development and angiogenesis in adult brain tumor: Glioblastoma. *Mol Neurobiol* 57: 2461-2478, 2020.
3. García-Romero N, Palacín-Aliana I, Madurga R, Carrión-Navarro J, Esteban-Rubio S, Jiménez B, Collazo A, Pérez-Rodríguez F, Ortiz de Mendivil A, Fernández-Carballal C, *et al.*: Bevacizumab dose adjustment to improve clinical outcomes of glioblastoma. *BMC Med* 18: 142, 2020.
4. Schulte JD, Aghi MK and Taylor JW: Anti-angiogenic therapies in the management of glioblastoma. *Chin Clin Oncol* 10: 37, 2021.
5. Staton CA, Brown NJ, Rodgers GR, Corke KP, Tazzyman S, Underwood JC and Lewis CE: Alphastatin, a 24-amino acid fragment of human fibrinogen, is a potent new inhibitor of activated endothelial cells in vitro and in vivo. *Blood* 103: 601-606, 2004.
6. Guo SW, Che HM and Li WZ: Anti-tumor effect of lentivirus-mediated gene transfer of alphastatin on human glioma. *Cancer Sci* 102: 1038-1044, 2011.
7. Quiñones JP, Peniche H and Peniche C: Chitosan based self-assembled nanoparticles in drug delivery. *Polymers (Basel)* 10: 235, 2018.
8. Yu H, Yang Z, Li F, Xu L and Sun Y: Cell-mediated targeting drugs delivery systems. *Drug Deliv* 27: 1425-1437, 2020.
9. Porada CD and Almeida-Porada G: Mesenchymal stem cells as therapeutics and vehicles for gene and drug delivery. *Adv Drug Deliv Rev* 62: 1156-1166, 2010.
10. Zhang J, Liu Y, Chen Y, Yuan L, Liu H, Wang J, Liu Q and Zhang Y: Adipose-derived stem cells: Current applications and future directions in the regeneration of multiple tissues. *Stem Cells Int* 2020: 8810813, 2020.
11. Kucerova L, Altanerova V, Matuskova M, Tyciakova S and Altaner C: Adipose tissue-derived human mesenchymal stem cells mediated prodrug cancer gene therapy. *Cancer Res* 67: 6304-6313, 2007.
12. Choi SA, Lee JY, Kwon SE, Wang KC, Phi JH, Choi JW, Jin X, Lim JY, Kim H and Kim SK: Human adipose tissue-derived mesenchymal stem cells target brain tumor-initiating cells. *PLoS One* 10: e0129292, 2015.
13. Liang C, Shangguan J, Yang L and Guo S: Downregulation of astrocyte elevated gene-1 expression inhibits the development of vasculogenic mimicry in gliomas. *Exp Ther Med* 21: 22, 2021.
14. Liang C, Guo S and Yang L: Effects of all-trans retinoic acid on VEGF and HIF-1 α expression in glioma cells under normoxia and hypoxia and its anti-angiogenic effect in an intracerebral glioma model. *Mol Med Rep* 10: 2713-2719, 2014.
15. Workman P, Aboagye EO, Balkwill F, Balmain A, Bruder G, Chaplin DJ, Double JA, Everitt J, Farningham DA, Glennie MJ, *et al.*: Guidelines for the welfare and use of animals in cancer research. *Br J Cancer* 102: 1555-1577, 2010.
16. Chen L, Li T, Li R, Wei B and Peng Z: Alphastatin downregulates vascular endothelial cells sphingosine kinase activity and suppresses tumor growth in nude mice bearing human gastric cancer xenografts. *World J Gastroenterol* 12: 4130-4136, 2006.
17. Staton CA, Stribbling SM, Garcia-Echeverria C, Bury JP, Tazzyman S, Lewis CE and Brown NJ: Identification of key residues involved in mediating the in vivo anti-tumor/anti-endothelial activity of alphastatin. *J Thromb Haemost* 5: 846-854, 2007.
18. Che H, Song J, Guo S, Wang W and Gao G: Inhibition of xenograft human glioma tumor growth by lentivirus-mediated gene transfer of alphastatin. *Oncol Rep* 29: 1101-1107, 2013.
19. Guo SW, Che HM and Li WZ: Construction of recombinant lentivirus vector for tumor vasoinhibitory peptide alphastatin gene delivery. *Mol Med Rep* 3: 923-928, 2010.
20. Meadows KN, Bryant P, Vincent PA and Pumiglia KM: Activated Ras induces a proangiogenic phenotype in primary endothelial cells. *Oncogene* 23: 192-200, 2004.
21. Carmeliet P and Collen D: Molecular basis of angiogenesis. Role of VEGF and VE-cadherin. *Ann N Y Acad Sci* 902: 249-264, 2000.
22. Chrifi I, Louzao-Martinez L, Brandt M, van Dijk CGM, Burgisser P, Zhu C, Kros JM, Duncker DJ and Cheng C: CMTM3 (CKLF-Like marvel transmembrane domain 3) mediates angiogenesis by regulating cell surface availability of VE-cadherin in endothelial adherens junctions. *Arterioscler Thromb Vasc Biol* 37: 1098-1114, 2017.
23. Duan HF, Wu CT, Lu Y, Wang H, Liu HJ, Zhang QW, Jia XX, Lu ZZ and Wang LS: Sphingosine kinase activation regulates hepatocyte growth factor induced migration of endothelial cells. *Exp Cell Res* 298: 593-601, 2004.
24. Shu X, Wu W, Mosteller RD and Broek D: Sphingosine kinase mediates vascular endothelial growth factor-induced activation of ras and mitogen-activated protein kinases. *Mol Cell Biol* 22: 7758-7768, 2002.
25. Wang XX, Sun RJ, Wu M, Li T, Zhang Y and Chen L: Differential protein expression in EC304 gastric cancer cells induced by alphastatin. *Asian Pac J Cancer Prev* 13: 1667-1674, 2012.
26. Feng Y, Gross S, Wolf NM, Butenschön VM, Qiu Y, Devraj K, Liebner S, Kroll J, Skolnik EY, Hammes HP and Wieland T: Nucleoside diphosphate kinase B regulates angiogenesis through modulation of vascular endothelial growth factor receptor type 2 and endothelial adherens junction proteins. *Arterioscler Thromb Vasc Biol* 34: 2292-2300, 2014.
27. Li Z, Huo X, Chen K, Yang F, Tan W, Zhang Q, Yu H, Li C, Zhou D, Chen H, *et al.*: Profilin 2 and endothelial exosomal profilin 2 promote angiogenesis and myocardial infarction repair in mice. *Front Cardiovasc Med* 9: 781753, 2022.
28. Huang B, Huang LF, Zhao L, Zeng Z, Wang X, Cao D, Yang L, Ye Z, Chen X, Liu B, *et al.*: Microvesicles (MIVs) secreted from adipose-derived stem cells (ADSCs) contain multiple microRNAs and promote the migration and invasion of endothelial cells. *Genes Dis* 7: 225-234, 2019.
29. Gangadaran P, Rajendran RL, Oh JM, Oh EJ, Hong CM, Chung HY, Lee J and Ahn BC: Identification of angiogenic cargo in extracellular vesicles secreted from human adipose tissue-derived stem cells and induction of angiogenesis in vitro and in vivo. *Pharmaceutics* 13: 495, 2021.
30. Pendleton C, Li Q, Chesler DA, Yuan K, Guerrero-Cazares H and Quinones-Hinojosa A: Mesenchymal stem cells derived from adipose tissue vs bone marrow: In vitro comparison of their tropism towards gliomas. *PLoS One* 8: e58198, 2013.
31. Chuang CC, Chen YN, Wang YY, Huang YC, Lin SY, Huang RY, Jang YY, Yang CC, Huang YF and Chang CW: Stem cell-based delivery of gold/chlorin e6 nanocomplexes for combined photothermal and photodynamic therapy. *ACS Appl Mater Interfaces* 12: 30021-30030, 2020.
32. Huang WC, Lu IL, Chiang WH, Lin YW, Tsai YC, Chen HH, Chang CW, Chiang CS and Chiu HC: Tumortropic adipose-derived stem cells carrying smart nanotherapeutics for targeted delivery and dual-modality therapy of orthotopic glioblastoma. *J Control Release* 254: 119-130, 2017.
33. Feng Y, Zhu M, Dangelmajer S, Lee YM, Wijesekera O, Castellanos CX, Denduluri A, Chaichana KL, Li Q, Zhang H, *et al.*: Hypoxia-cultured human adipose-derived mesenchymal stem cells are non-oncogenic and have enhanced viability, motility, and tropism to brain cancer. *Cell Death Dis* 5: e1567, 2014.
34. Heddleston JM, Hitomi M, Venere M, Flavahan WA, Yang K, Kim Y, Minhas S, Rich JN and Hjelmeland AB: Glioma stem cell maintenance: The role of the microenvironment. *Curr Pharm Des* 17: 2386-2401, 2011.
35. Schiffer D, Annovazzi L, Casalone C, Corona C and Mellai M: Glioblastoma: Microenvironment and niche concept. *Cancers (Basel)* 11: 5, 2018.
36. Calabrese C, Poppleton H, Kocak M, Hogg TL, Fuller C, Hamner B, Oh EY, Gaber MW, Finklestein D, Allen M, *et al.*: A perivascular niche for brain tumor stem cells. *Cancer Cell* 11: 69-82, 2007.
37. Peng L, Ming Y, Zhang L, Zhou J, Xiang W, Zeng S, He H and Chen L: MicroRNA-30a suppresses self-renewal and tumorigenicity of glioma stem cells by blocking the NT5E-dependent Akt signaling pathway. *FASEB J* 34: 5128-5143, 2020.



Copyright © 2023 Liang *et al.* This work is licensed under a Creative Commons Attribution-NonCommercial-NoDerivatives 4.0 International (CC BY-NC-ND 4.0) License.